



High-pressure dielectric behavior of polycrystalline CaMoO_4 : The role of grain boundaries



Tianru Qin ^a, Qinglin Wang ^b, Donghui Yue ^a, Wenshu Shen ^a, Yalan Yan ^a, Yonghao Han ^a, Yanzhang Ma ^{c,d}, Chunxiao Gao ^{a,*}

HPSTAR
545-2018

^a State Key Laboratory of Superhard Materials, Jilin University, Changchun, 130012, China

^b Shandong Key Laboratory of Optical Communication Science and Technology, School of Physics Science & Information Technology, Liaocheng University, Liaocheng, 252059, China

^c Department of Mechanical Engineering, Texas Tech University, Lubbock, TX, 79409, USA

^d Center for High Pressure Science & Technology Advanced Research, Changchun, 130012, China

ARTICLE INFO

Article history:

Received 12 July 2017

Received in revised form

25 September 2017

Accepted 26 September 2017

Available online 28 September 2017

Keywords:

CaMoO_4

High pressure

Dielectric properties

Grain boundary

ABSTRACT

The dielectric behavior of polycrystalline CaMoO_4 was investigated at pressures up to 36.0 GPa using *in situ* impedance measurements. Grain boundaries played a dominant role in the electrical transport process. Grain boundary microstructures rearranged with the application of pressures, and the relaxation activation energy increased with increasing pressure in the tetragonal phase but decreased in the monoclinic phase. The variation of the bulk resistance with pressure was attributed to defects generated during the compression. The increasing grain boundary resistance with pressure in the tetragonal phase was caused by the increased number of dangling bonds. In the tetragonal phase, localization around O atoms weakened with increasing pressure, which promoted the polarization of Mo–O electric dipoles and led to an increase of the relative dielectric constant. In addition, the dielectric loss tangent of CaMoO_4 was significantly reduced in the low frequency range after a pressure cycle. This work demonstrates that regulation of the polycrystalline dielectric performance by modifying the grain boundary distribution under compression can be used as an effective method to improve the bulk properties of ABO_4 -type dielectrics.

© 2017 Elsevier B.V. All rights reserved.

1. Introduction

With increasing resource requirements, scheelite-structured molybdates have received considerable attention as a new type of functional material for a wide range of applications [1–4]. Calcium molybdate (CaMoO_4) is a representative example; at ambient conditions, its Ca atom exhibits eight-fold oxygen coordination, and the Mo atom forms a MoO_4^{2-} tetrahedron. This special structure endows CaMoO_4 with excellent properties, such as good thermal chemical stability and eminent luminescence properties, leading to its wide application in white light emitting diodes, displays, and devices in photochemical fields [5–8]. CaMoO_4 is also a potential candidate for microwave dielectric devices that require materials with low permittivity and high quality factors, such as dielectric resonators [9,10]. In addition, CaMoO_4 is an excellent host material

for various rare-earth ions. By controlling the type and concentration of doped ions, the luminescent color and efficiency of CaMoO_4 can be modified, providing a foundation for different optical CaMoO_4 -based applications [11,12].

In addition to doping, the external parameters of temperature and pressure also provide powerful means to tune the structure and properties of materials [13]. Previous investigations have revealed that scheelite-structured CaMoO_4 exhibits good structural stability at extremely high and low temperatures (6 K–1300 K) [5,6]; however, structural phase transitions occur under compression. Nicol et al. first reported an unknown pressure-induced phase transition in single crystal CaMoO_4 starting at 2.7 GPa based on Raman scattering for pressures up to 4 GPa [14]. However, using X-ray diffraction analysis, Hazen et al. showed that no reversible phase transitions occurred in single crystal CaMoO_4 up to 6 GPa and that significant structural changes occurred in the eight-coordinated site, which changed more parallel to *c* than perpendicular to *c* with changes in pressure [15]. Another room-temperature Raman scattering study of single crystal CaMoO_4

* Corresponding author.

E-mail address: cc060109@qq.com (C. Gao).

was performed by Christofilos et al., and the experimental pressure was extended to 23 GPa [16]. These authors concluded that the single crystal CaMoO_4 underwent two phase transitions at 8.2 and 15 GPa.

Compared with single crystals, polycrystals contain many grain boundaries, and the structures and properties are affected by both the grains and grain boundaries. Hence, the pressure effects on the structural properties of polycrystals could differ. For example, using Raman experiments, Breiteringer et al. observed that no phase transitions occurred in polycrystalline CaMoO_4 up to 3 GPa [17]. Then, combining X-ray diffraction experiments with General Structure Analysis System (GSAS) software, Crichton et al. uncovered the phase transition of polycrystalline CaMoO_4 from its initial tetragonal phase to a monoclinic phase at 15 GPa [18]. The structural behaviors of polycrystalline CaMoO_4 thus differ from those of its single crystal counterpart under compression, which is related to the grain boundary effect.

In addition to driving materials toward higher-density structures and tuning the intra- and intermolecular structures, pressure can also regulate the electrical transport properties of materials [19,20]. However, the understanding of the pressure effect on the electrical behavior of CaMoO_4 , such as the relaxation process, complex dielectric properties, and effect of electric field and pressure on the electrical polarization and motion of bound charges, remains rather limited. Unlike their single crystalline counterparts, polycrystalline materials contain a large number of grain boundaries, which result in special properties. Grain boundaries are generally produced by some interaction between neighboring grains, which can improve the initial performance of bulk materials or even generate properties that cannot be achieved by individual grain. Therefore, the interaction of grains across a grain boundary can be a source of desirable bulk properties if the grain boundaries are properly designed and controlled. It is thus worthwhile to explore the effects of grain boundaries on the transport and dielectric properties of materials. Therefore, a systematic study of the high-pressure dielectric behavior of polycrystalline CaMoO_4 is necessary.

In this work, we conducted *in situ* alternate-current (AC) impedance spectra measurements in a diamond anvil cell (DAC) at pressures up to 36.0 GPa to obtain a comprehensive understanding of the dielectric behavior of polycrystalline CaMoO_4 under compression. The contributions of bulk and grain boundary effects on the electrical transport processes are distinguished, and the relaxation frequency, complex dielectric constant, modulus, and dielectric loss of CaMoO_4 under compression are also discussed. In addition, the first-principles calculations were performed to obtain a better understanding of the electronic transport behavior of CaMoO_4 under compression.

2. Experimental and theoretical methods

Polycrystalline CaMoO_4 powder was purchased from Alfa Aesar Co. with a purity of 99.9965%. The sample initially exhibited a tetragonal structure with space group $I4_1/a$, which was verified by X-ray diffraction measurements, as shown in Fig. S1 in the supplementary material. A DAC was used to conduct high pressure experiments. The impedance measurements were performed using a Solartron 1260 impedance analyzer equipped with Solartron 1296 dielectric interface. The parallel-plate electrodes configuration was selected for the AC impedance spectra measurements, and the fabrication process for the detecting microcircuit on diamond anvils is described in our previous works [21–23]. A sine voltage signal with an amplitude of 1.0 V was applied to the sample. To ensure the accuracy of the electrical measurements, no pressure transmitting medium was introduced. Ruby fluorescence was used

as a pressure scale for pressure calibration [24]. The sample thickness under compression was measured with a micrometer [25].

The first-principles calculations were performed based on the density functional theory and the pseudo potential method on the standard CASTEP program in the Material Studio package [26]. The electron–ion interaction was described by Vanderbilt-type ultrasoft pseudopotentials [27]. The exchange and correlation terms were described using the generalized gradient approximation (GGA) in the scheme of Perdew–Burke–Ernzerhof (PBE) parameterization [28]. The geometric optimization of the unit cell was conducted with the Broyden–Fletcher–Goldfarb–Shanno (BFGS) minimization algorithm. Integration in the Brillouin zone was performed using special k points generated with $7 \times 7 \times 9$ and $7 \times 3 \times 7$ mesh parameter grids for the tetragonal and monoclinic phases, respectively. A plane-wave cutoff energy of 540 eV was set up for the two phases to guarantee the convergence of the enthalpy calculations.

3. Results and discussion

The $Z''-Z'$ impedance spectra of CaMoO_4 under various pressures are presented in Fig. 1(a)–(c). Each spectrum includes two semicircular arcs: one is large and clear, and the another is small but visible, as shown in the insets. The left small arc represents the bulk conduction in the high frequency region, and the right large one in the low frequency region corresponds to the grain boundary conduction. The frequency dependence of the imaginary part $Z''-f$ of CaMoO_4 under different pressures is shown in Fig. 1(d)–(f). The relaxation peak at low frequency corresponds to the grain boundary conduction of CaMoO_4 . The position and intensity of the relaxation peak describe the electrical relaxation processes occurring in CaMoO_4 . The relaxation frequency corresponds to the imaginary impedance peak and equals the reciprocal of the time constant. The weakening of the relaxation peak indicates that the relaxation process of the grain boundary is impeded.

Considering that large differences existed between the bulk and grain boundary conduction ($f_b \gg f_{gb}$), we adopted the alternative representation $Z'-Z''/f$ to process the impedance data of CaMoO_4 ,

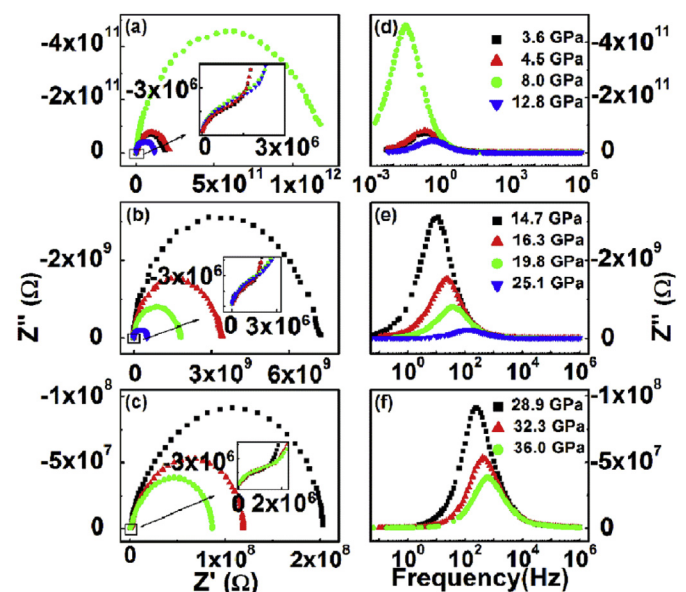


Fig. 1. (a)–(c) The impedance spectra $Z''-Z'$ and (d)–(f) the frequency dependence of imaginary part of $Z''-f$ plots of CaMoO_4 under compression. Inset: enlargement of impedance spectra in high frequency region.

following the report of Abrantes et al. [29], and the results are presented in Fig. 2. Three different straight-line segments appeared in the $Z''-Z''/f$ plots, corresponding to the properties of the bulk, grain boundary, and electrode from left to right. The relevant electrical parameters of the bulk, grain boundary, and electrode were obtained by calculating the corresponding slopes and intercepts of the different regions. Thus, the effect of pressure on the dielectric properties of CaMoO_4 could be quantified. The electrode relaxation frequency was close to 0 Hz over the entire pressure range, which explain the absence of the third impedance arc related to the electrode in the low frequency region; therefore, the effect of electrodes can be ignored in this work.

The variations of the electrical resistance and relaxation frequency of the bulk and grain boundary (R_b , R_{gb} , f_b , f_{gb}) and total resistance (R_T) as a function of pressure are presented in Fig. 3. R_T designates the total measured resistance, namely $R_T = R_b + R_{gb}$. Because no pressure transmission medium was used in the electrical experiments, the deviatoric stresses under non-hydrostatic condition resulted in the phase transition pressure point shifting to lower pressure than that reported in previous X-ray diffraction experiments [30]. In addition, the grain boundary effect in a polycrystalline sample can also affect the transition points, which always differ from those in single crystals. The inflection point at 8.0 GPa of the electrical parameters represents the beginning of the structural phase transition from the tetragonal to monoclinic phase, which is completed at 13.9 GPa. That is, from 8.0 to 13.9 GPa, the low- and high-pressure phases coexist in CaMoO_4 under non-hydrostatic conditions.

To better study the effect of the grain boundaries on the electrical properties, samples quenched from different pressures were investigated using high-resolution transmission electron microscopy (HRTEM). HRTEM images of the samples are presented in Fig. 4. The average grain size of the CaMoO_4 particles decreased significantly from ambient pressure to 7 GPa, indicating that the density of grain boundaries increased with increasing pressure. The increase in grain size in Fig. 4(c) compared with that in Fig. 4(b) indicates that the grains grew during the transition. Upon increasing the pressure to 36 GPa, the grains became slightly larger than at 16 GPa, as observed in Fig. 4(d) indicating that the density of grain boundaries gradually decreased after the phase transition.

As observed in Fig. 3(b), in the tetragonal phase, R_{gb} gradually increased with increasing pressure; this phenomenon results from the breakdown of the grains with increasing pressure, generating additional dangling bonds. The dangling bonds can capture more electrons and lead to the increase of R_{gb} with increasing pressure. Accordingly, the grain boundary relaxation time increases with increasing pressure, which is consistent with the decreasing trend of f_{gb} , as observed in Fig. 3(c). In the monoclinic phase (from 13.9 to 36 GPa), the density of grain boundaries gradually decreased with increasing pressure, indicating that the number of dangling bonds

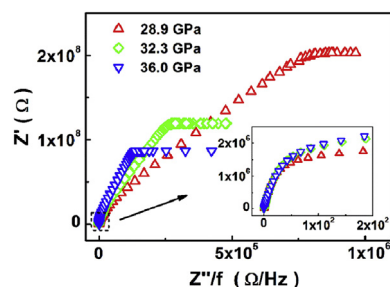


Fig. 2. $Z''-Z''/f$ plots of CaMoO_4 at several pressures. Inset: enlargement of high frequency region.

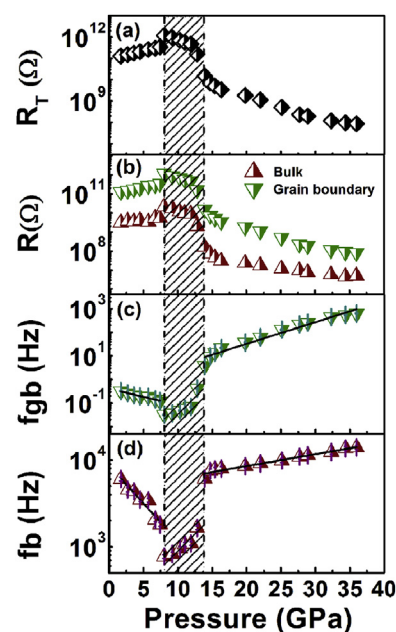


Fig. 3. (a, b) Pressure dependence of total resistance ($R_T = R_b + R_{gb}$), bulk and grain boundary resistance (R_b , R_{gb}) of CaMoO_4 . (c, d) Pressure dependence of grain boundary and bulk relaxation frequency (f_{gb} , f_b) of CaMoO_4 .

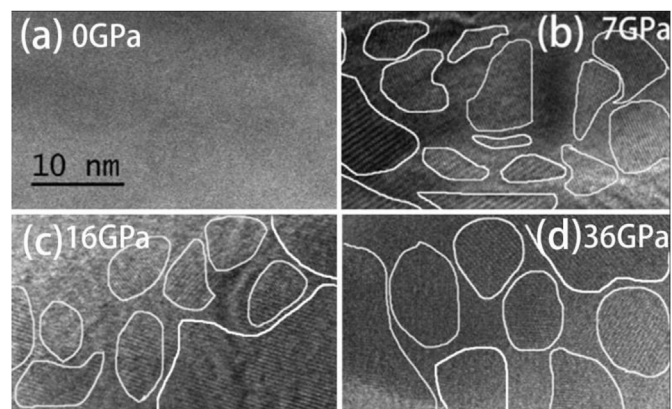


Fig. 4. High-resolution transmission electron microscopy (HRTEM) images of CaMoO_4 quenched from different pressures: (a) ambient pressure, (b) 7 GPa, (c) 16 GPa and (d) 36 GPa.

at the grain boundary gradually decreased and, thus, that the number of electrons captured by dangling bonds decreased. As a result, R_{gb} decreased with increasing pressure. Meanwhile, the reduction of dangling bonds strengthened the grain boundaries, resulting in an increase of f_{gb} with increasing pressure in the monoclinic phase. The specific reasons for the variation of R_b will be discussed in combination with theoretical calculations later.

The bulk relaxation frequency represents the charge–discharge rate in the dipole oscillation process, and the relaxation activation energy (E) presents the energy to activate the resonance. The pressure dependence of E can be obtained by linear fitting of $\ln f_b - P$ according to the following Arrhenius relationship:

$$d(\ln f_b)/dP = -1/k_B T (dE/dP), \quad (1)$$

where k_B represents the Boltzmann constant and T is the temperature. The variation rates of E along with pressure in the tetragonal

and monoclinic phases were calculated to be 5.14 and -0.35 meV/GPa, respectively. The positive value of dE/dP in the tetragonal phase indicates that the vibration damping of Mo–O dipoles is strengthened with increasing pressure and that the charge–discharge process becomes harder. In contrast, in the monoclinic phase, the charge–discharge process becomes much easier with increasing pressure.

The bulk dielectric constant (ϵ_r) of CaMoO_4 can be obtained using Eq. (2):

$$\epsilon_r(P) = d / (2\pi R_b \epsilon_0 f_b S), \quad (2)$$

where d represents the thickness of the sample, ϵ_0 is the vacuum permittivity, and S is the area of the electrode. The pressure dependence of ϵ_r is shown in Fig. 5(a). A discontinuous change of ϵ_r occurred near 8 GPa, which can be attributed to the pressure-induced structural phase transitions. ϵ_r increases with increasing pressure in the tetragonal phase, indicating that the electric polarization is strengthened with increasing pressure in the external electric field. In contrast, in the monoclinic phase, ϵ_r increases more slowly.

To obtain a better understanding of the dielectric properties of CaMoO_4 , the complex dielectric constant (ϵ' , ϵ'') and dielectric loss tangent ($\tan\delta$) were evaluated as a function of frequency under compression and the results are presented in Fig. 5(b)–(f). The dispersion in ϵ' versus f weakens with increasing pressure. The decreasing ϵ' with increasing frequency below 10^5 Hz is due to the turning-direction polarization of the intrinsic electric dipoles behind the changing external electric field; only parts of dipoles can catch up with the changing external electric field. The decreasing number of polarized dipoles led to a decreasing ϵ' with increasing frequency. At $\sim 10^5$ Hz, ϵ' reduced to a new constant

value, and ϵ'' became 0, indicating that the polarization of the intrinsic electric dipoles have no response to the external electric field.

When an external electric field was applied to the materials, the relaxations of polarization and conduction caused energy loss. As observed in Fig. 5(d), the loss tangent ($\tan\delta$) of CaMoO_4 decreased with increasing frequency over the entire pressure range. The transport direction of electron motion changed more frequently with increasing frequency, which weakened the dipole polarization. Fig. 5(e) shows the variation of $\tan\delta$ as a function of pressure at 10^{-1} Hz; the value increased rapidly with increasing pressure up to 36.0 GPa. However, compared with that at 1.7 GPa during compression, $\tan\delta$ was significantly reduced in the low frequency region when the pressure was reduced to 1.8 GPa, indicating that the dielectric properties of CaMoO_4 can be effectively improved after a pressure cycle.

Fig. 5 depicts a relaxation process, as demonstrated by the gradual decrease in ϵ' and the broad peak in $\tan\delta$. Note that a very large dielectric constant was observed at low frequencies, suggesting strong dielectric relaxation. The observed high dielectric permittivity is a typical product of increased interfacial polarization between grain boundaries at low frequencies in the samples, such as in $\text{CaCu}_3\text{Ti}_4\text{O}_{12}$ [31]. The $\tan\delta$ peaks exhibit distributions of Debye-like relaxation processes, and are consistent with the Maxwell–Wagner relaxation model.

Complex modulus plots are particularly useful to understand the relaxation behavior, because the $Z'-f$ plots highlight phenomena characterized by large resistance, whereas $M''-f$ plots identify electrical responses with small capacitance [32]. The complex electric modulus is plotted as a function of frequency at different pressures in Fig. 6(a) and (b). The two peaks in the $M''-f$ plots indicate that two types of electrical response mechanism existed in CaMoO_4 . The change of the two peaks in M'' versus f under compression is shown in Fig. 6(b), which supports the occurrence of a relaxation process. M''_{\max} (the maximum value of the two peaks) is the reciprocal of the relaxation time. The peak corresponding to the grain boundary (in the low frequency region) first shifted toward lower frequencies and then toward higher frequencies with increasing pressure. Therefore, the relaxation rate in the grain boundary first decreased and then increased with increasing pressure. The peak corresponding to the bulk (in the high frequency region) exhibited a similar changing trend with the grain boundary. In addition, the peak reveals the change from long-range to short-range mobility with increasing frequency.

To further analyze the dielectric properties of CaMoO_4 under compression, we performed the first-principles band structure and the charge density difference calculations up to 36.0 GPa. The band

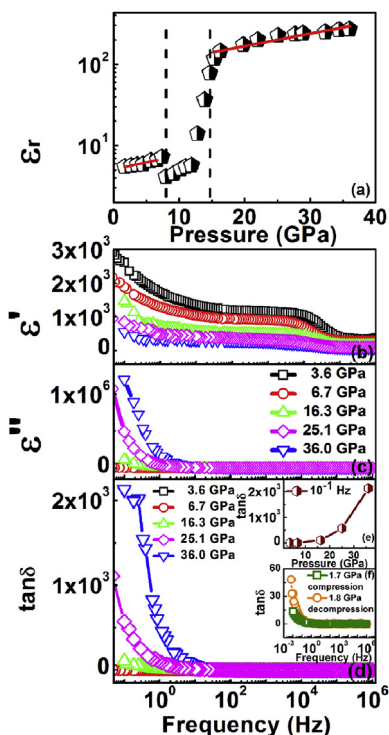


Fig. 5. (a) Pressure dependence of relative permittivity of CaMoO_4 . (b, c) Frequency dependence of real and imaginary parts of complex permittivity for CaMoO_4 at selected pressures. (d) Dielectric loss factor ($\tan\delta$) versus frequency of CaMoO_4 at representative pressures. Inset: (e) loss tangent versus pressure at a low frequency of 10^{-1} Hz and (f) loss tangent at 1.7 and 1.8 GPa after pressure release.

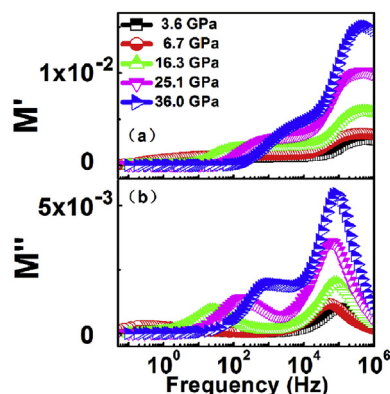


Fig. 6. Frequency dependence of (a) M' and (b) M'' of CaMoO_4 at different pressures.

gap (E_g) of CaMoO_4 under ambient conditions was 3.36 eV, which is consistent with previous reports (3.41 eV) [33]. E_g of CaMoO_4 decreased with increasing pressure in both the tetragonal and monoclinic phases, and the dE_g/dP values were -6.12 and -0.41 meV GPa^{-1} , respectively. E_g of CaMoO_4 was weakly dependent on pressure, which is similar to the findings for CaWO_4 [34]. Comparison of dE_g/dP and $d(\ln R)/dP$ did not satisfy the Arrhenius relationship (see supplementary material for further details). Therefore, the defects generated during compression play a vital role in the electron conduction. The concentration and variety of defects increased with increasing pressure and the carrier scattering effects were enhanced, increasing R_b . The charge density difference maps at different pressures are presented in Fig. 7. Charge distribution transfer occurred from Mo^{6+} to O^{2-} ions in the tetragonal and monoclinic phases. In the tetragonal phase, the electron localization around O atoms decreased with increasing pressure, and the polarization of Mo–O electric dipoles became easier, leading to the increase of ϵ_r with pressure. However, in the monoclinic phase, the electron localization around O atoms increased with increasing pressure, and the polarization of Mo–O electric dipoles became harder. In addition to the polarization, the microstructure (grain size and grain boundary state) can affect the relative dielectric constant. Therefore, the increasing ϵ_r with pressure in the monoclinic phase is mainly attributed to the variation of microstructure.

Compared with BaMoO_4 [35], the grain boundary effect plays a dominant role in the electrical transport process of CaMoO_4 . R_T of CaMoO_4 decreased by 5 orders of magnitude at a pressure of 36 GPa, whereas the resistance of BaMoO_4 changed by one order of magnitude, indicating that pressure has a stronger regulating effect on CaMoO_4 . In contrast to BaMoO_4 , the relative dielectric constant of CaMoO_4 increased with compression, indicating that the charge storage capacity enhanced with pressure. Note that the dielectric loss of CaMoO_4 also significantly decreases in the low frequency after a pressure cycle, similar to that of BaMoO_4 . In addition, SrMoO_4 has the same initial and high-pressure structures as BaMoO_4 and CaMoO_4 [36]. Therefore, it can be speculated that the

grain boundaries in polycrystalline SrMoO_4 should also play an important role in its transport properties and may also improve the bulk dielectric performance, such as in BaMoO_4 and CaMoO_4 . Detailed investigation on the dielectric properties of SrMoO_4 and MgMoO_4 will be conducted in future works, which will help provide a basic understanding of ABO_4 -type materials and their applications.

4. Conclusions

In summary, the high pressure dielectric properties of CaMoO_4 for pressures up to 36.0 GPa were investigated by combining *in situ* impedance spectra measurements and first-principles calculations. The anomalous inflection points in the electrical parameters were related to pressure-induced structural phase transitions, and the grain boundary effect was observed to dominate the electrical transport process. The density of grain boundaries changed as a function of pressure, with rearrangement of the grain boundary microstructure. The increasing grain boundary resistance with pressure in the tetragonal phase was caused by the increased number of dangling bonds. The relaxation activation energy increased with increasing pressure in the tetragonal phase but decreased in the monoclinic phase. The increase of the relative dielectric constant with pressure in the tetragonal phase was attributed to the weakened localization around O atoms. In addition, the dispersion in ϵ' versus f weakened with increasing pressure. The dielectric loss significantly decreased in the low frequency region after a pressure cycle, indicating that the dielectric performance of CaMoO_4 can be effectively improved with compression.

Acknowledgements

This work was supported by the National Natural Science Foundation of China (Grant No. 11374121, 11404133 and 11604133), the Program of Science and Technology Development Plan of Jilin Province (Grant No. 20140520105JH), the Open Project of State Key Laboratory of Superhard Materials (Jilin University, Grant No. 201612), and the Initial Foundation for Doctor Programme of Liaocheng University (Grant No. 318051610).

Appendix A. Supplementary data

Supplementary data related to this article can be found at <https://doi.org/10.1016/j.jallcom.2017.09.286>.

References

- [1] G.M. Gurgel, L.X. Lovisa, O.L.A. Conceição, M.S. Li, E. Longo, C.A. Paskocimas, F.V. Motta, M.R.D. Bomio, Evaluation of morphology and photoluminescent properties of PbMoO_4 crystals by ultrasonic amplitude, *J. Mater. Sci.* 52 (2016) 4608–4620.
- [2] R. Karthik, N. Karikalan, S.-M. Chen, J. Vinoth Kumar, C. Karupiah, V. Muthuraj, Assessment of divergent functional properties of seed-like strontium molybdate for the photocatalysis and electrocatalysis of the post-harvest scald inhibitor diphenylamine, *J. Catal.* 352 (2017) 606–616.
- [3] X. Ma, W. Zhao, J. Wu, X. Jia, Preparation of flower-like BaMoO_4 and application in rechargeable lithium and sodium ion batteries, *Mater. Lett.* 188 (2017) 248–251.
- [4] D.A. Spassky, N.S. Kozlova, V. Nagirnyi, A.E. Savon, Y.A. Hizhnyi, S.G. Nedilko, Excitation energy transfer to luminescence centers in $\text{M}^{\text{II}}\text{MoO}_4$ ($\text{M}^{\text{II}}=\text{Ca}, \text{Sr}, \text{Zn}, \text{Pb}$) and Li_2MoO_4 , *J. Lumin.* 186 (2017) 229–237.
- [5] A.E. Musikhin, V.N. Naumov, M.A. Bespyatov, V.N. Shlegel, Heat capacity and thermodynamic functions of CaMoO_4 at low temperatures, *J. Alloys Compd.* 655 (2016) 165–171.
- [6] E. Sarantopoulou, C. Raptis, S. Ves, D. Christofilos, G.A. Kourouklis, Temperature and pressure dependence of Raman-active phonons of CaMoO_4 : an anharmonicity study, *J. Phys. Condens. Matter* 14 (2002) 8925–8938.
- [7] Y. Han, L. Wang, D. Wang, D. Liang, S. Wang, G. Lu, Z. Di, G. Jia, Lanthanide ions-doped calcium molybdate pie-like microstructures: synthesis, structure

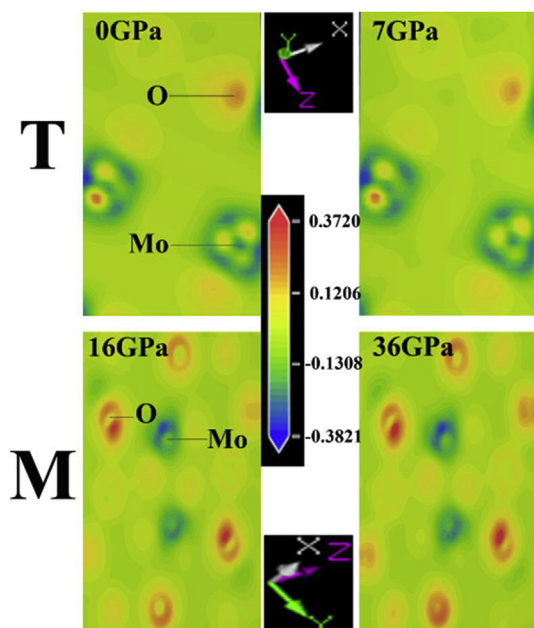


Fig. 7. Calculated charge density difference maps through the Mo and O atoms with an isosurface value of 0.1 for the tetragonal (T) phase (0, 7 GPa) and monoclinic (M) phase (16, 36 GPa).

- characterization, and luminescent properties, *J. Alloys Compd.* 695 (2017) 3018–3023.
- [8] M. Laguna, N.O. Nuñez, A.I. Becerro, M. Ocaña, Morphology control of uniform CaMoO₄ microarchitectures and development of white light emitting phosphors by Ln doping (Ln = Dy³⁺, Eu³⁺), *CrystEngComm* 19 (2017) 1590–1600.
- [9] G.-K. Choi, J.-R. Kim, S.H. Yoon, K.S. Hong, Microwave dielectric properties of scheelite (A=Ca, Sr, Ba) and wolframite (A=Mg, Zn, Mn) AMoO₄ compounds, *J. Eur. Ceram. Soc.* 27 (2007) 3063–3067.
- [10] X. Wang, T. Chen, M. Li, B. Ding, Y. Liu, H. Zhang, J. Liao, Preparation and characteristics of polyimide/CaMoO₄ nanocomposites with enhanced dielectric performance and thermal stability, *J. Mater. Sci. Mater. Electron.* 28 (2017) 5215–5221.
- [11] X. Ming, Q. Meng, J. Xiong, W. Sun, Study on the color tunability and energy transfer mechanism in Tb³⁺, Sm³⁺ co-doped CaMoO₄ phosphors, *J. Alloys Compd.* 695 (2017) 1691–1698.
- [12] Y. Zhai, Y. Han, W. Zhang, Y. Yin, X. Zhao, J. Wang, X. Liu, Influence of doping alkali metal ions on the structure and luminescent properties of microwave synthesized CaMoO₄:Dy³⁺ phosphors, *J. Alloys Compd.* 688 (2016) 241–247.
- [13] S.S. Krishnopenko, I. Yahniuk, D.B. But, V.I. Gavrilenko, W. Knap, F. Teppe, Pressure- and temperature-driven phase transitions in HgTe quantum wells, *Phys. Rev. B* 94 (2016) 245402.
- [14] M. Nicol, J.F. Durana, Vibrational raman spectra of CaMoO₄ and CaWO₄ at high pressures, *J. Chem. Phys.* 54 (1971) 1436–1440.
- [15] R.M. Hazen, L.W. Finger, J.W.E. Mariathasan, High-pressure crystal chemistry of scheelite-type tungstates and molybdates, *J. Phys. Chem. Solids* 46 (1985) 253–263.
- [16] D. Christofilos, G.A. Kourouklis, S. Ves, A high pressure raman study of calcium molybdate, *J. Phys. Chem. Solids* 56 (1995) 1125–1129.
- [17] D.K. Breiting, L. Emmert, W. Kress, High-pressure raman studies of scheelites and related solids, *Ber. Bunsenges. Phys. Chem.* 85 (1981) 504–505.
- [18] W.A. Crichton, A. Grzechnik, Crystal structure of calcium molybdate, CaMoO₄, a scheelite-type to fergusonite-type transition in powellite at P > 15 GPa, *Z. Kristallogr.- New Cryst. Struct.* 219 (2004) 369–370.
- [19] Q. Wang, Y. Han, C. Liu, Y. Ma, W. Ren, C. Gao, High-pressure electrical transport properties of KNbO₃: experimental and theoretical approaches, *Appl. Phys. Lett.* 100 (2012) 172905.
- [20] F. Ke, H. Dong, Y. Chen, J. Zhang, C. Liu, J. Zhang, Y. Gan, Y. Han, Z. Chen, C. Gao, J. Wen, W. Yang, X.J. Chen, V.V. Struzhkin, H.K. Mao, B. Chen, Decompression-Driven superconductivity enhancement in In₂Se₃, *Adv. Mater.* 29 (2017) 1701983.
- [21] Q. Wang, C. Liu, Y. Gao, Y. Ma, Y. Han, C. Gao, Mixed conduction and grain boundary effect in lithium niobate under high pressure, *Appl. Phys. Lett.* 106 (2015) 132902.
- [22] Y. Li, Y. Gao, Y. Han, C. Liu, W. Ren, Q. Wang, Y. Ma, B. Wu, C. Gao, Electrical transport properties of BaWO₄ under high pressure, *J. Phys. Chem. C* 116 (2012) 25198–25205.
- [23] Y. Wang, Y. Han, C. Gao, Y. Ma, C. Liu, G. Peng, B. Wu, B. Liu, T. Hu, X. Cui, W. Ren, Y. Li, N. Su, H. Liu, G. Zou, In situ impedance measurements in diamond anvil cell under high pressure, *Rev. Sci. Instrum.* 81 (2010) 013904.
- [24] G.J. Piermarini, S. Block, J.D. Barnett, R.A. Forman, Calibration of the pressure dependence of the R₁ ruby fluorescence line to 195 kbar, *J. Appl. Phys.* 46 (1975) 2774–2780.
- [25] M. Li, C. Gao, G. Peng, C. He, A. Hao, X. Huang, D. Zhang, C. Yu, Y. Ma, G. Zou, Thickness measurement of sample in diamond anvil cell, *Rev. Sci. Instrum.* 78 (2007) 075106.
- [26] M.D. Segall, P.J.D. Lindan, M.J. Probert, C.J. Pickard, P.J. Hasnip, S.J. Clark, M.C. Payne, First-principles simulation: ideas, illustrations and the CASTEP code, *J. Phys. Condens. Matter* 14 (2002) 2717–2744.
- [27] D. Vanderbilt, Soft self-consistent pseudopotentials in a generalized eigenvalue formalism, *Phys. Rev. B* 41 (1990) 7892–7895.
- [28] J.P. Perdew, K. Burke, M. Ernzerhof, Generalized gradient approximation made simple, *Phys. Rev. Lett.* 77 (1996) 3865–3868.
- [29] J.C.C. Abrantes, J.A. Labrincha, J.R. Frade, An alternative representation of impedance spectra of ceramics, *Mater. Res. Bull.* 35 (2000) 727–740.
- [30] D. Errandonea, Exploring the properties of MTO₄ compounds using high-pressure powder x-ray diffraction, *Cryst. Res. Technol.* 50 (2015) 729–736.
- [31] J.L. Zhang, P. Zheng, C.L. Wang, M.L. Zhao, J.C. Li, J.F. Wang, Dielectric dispersion of CaCu₃Ti₄O₁₂ ceramics at high temperatures, *Appl. Phys. Lett.* 87 (2005) 142901.
- [32] D.C. Sinclair, A.R. West, Impedance and modulus spectroscopy of semi-conducting BaTiO₃ showing positive temperature coefficient of resistance, *J. Appl. Phys.* 66 (1989) 3850–3856.
- [33] Y. Zhang, N.A.W. Holzwarth, R.T. Williams, Electronic band structures of the scheelite materials CaMoO₄, CaWO₄, PbMoO₄, and PbWO₄, *Phys. Rev. B* 57 (1998), 75576–12750.
- [34] R. Lacomba-Perales, D. Errandonea, A. Segura, J. Ruiz-Fuertes, P. Rodríguez-Hernández, S. Radescu, J. López-Solano, A. Mujica, A. Muñoz, A combined high-pressure experimental and theoretical study of the electronic band-structure of scheelite-type AWO₄ (A=Ca, Sr, Ba, Pb) compounds, *J. Appl. Phys.* 110 (2011) 043703.
- [35] T. Qin, Q. Wang, L. Wang, H. Yan, C. Liu, Y. Han, Y. Ma, C. Gao, High-pressure dielectric behavior of BaMoO₄: a combined experimental and theoretical study, *Phys. Chem. Chem. Phys.* 18 (2016) 33109–33114.
- [36] D. Errandonea, R.S. Kumar, X. Ma, C. Tu, High-pressure X-ray diffraction study of SrMoO₄ and pressure-induced structural changes, *J. Solid State Chem.* 181 (2008) 355–364.